ANALYZING EXPANDING CLAYS BY THERMOPOROMETRY USING A STOCHASTIC DECONVOLUTION OF THE DSC SIGNAL

Tomasz Kozlowski* and Łukasz Walaszczyk

Kielce University of Technology, Al. Tysiąclecia Państwa Polskiego 7, 25-314 Kielce, Poland

Abstract—A version of thermoporometry dedicated to analyzing the pore network of expanding clays is proposed here. The blurred, wide Differential Scanning Calorimetry (DSC) peak obtained upon the melting of a frozen clay sample is processed by means of a deconvolution analysis based on searching for such a temperature distribution of "pulse-like heat events" which, convolved with the apparatus function, gives a minimal deviation from the observed heat flux function, *i.e.* the calorimetric signal. As a result, a sharp thermogram was obtained which can be transformed easily into the pore-size distribution curve. Results obtained for samples of two Clay Minerals Society Source Clays (montmorillonites SWy-2 from Wyoming and STx-1b from Texas) at different water contents indicate a greater resolution and sensitivity than that achieved by classical thermoporometry using the unprocessed DSC signal. Phenomena corresponding to the evolution of the pore network as a function of the water content have been detected in samples with large water contents subjected to free drying prior to the experiments.

Key Words—Bentonites, Desmearing, Differential Scanning Calorimetry, Montmorillonite, Pore-size Distribution, Source Clays, STx-1b, SWy-2, Thermoporometry.

INTRODUCTION

Modeling of the processes of adsorption and filtration in clays is impossible without analysis on a microstructural level. Detailed studies have shown that the fluid-transport characteristics of such materials are mainly affected by the pore-size distribution (Velde *et al.*, 1996). Changes in the pore space induced by the swelling-shrinkage process in swelling clays are, however, a serious challenge in the predictive modeling of the hydraulic properties of such soils.

Bentonites, *i.e.* expanding clays consisting mostly of montmorillonite, are used in the stabilization of drill holes and in deep trenches for slurry walls. Bentonites have also been proposed as a barrier in the storage of nuclear waste (Montes *et al.*, 2003; Yang *et al.*, 2006). Bentonites are also used as environmental sealants, as waste-water treatment agents, as adsorbents of oil and grease, as a binding agent in the making of molding sands, as filtration media in the production of edible oils, and in many other ways (Gates *et al.*, 2009). Clays are used increasingly as a blank for the production of hybrid organic-inorganic composites (Carrado and Komadel, 2009). The need to remove toxic compounds from the environment and to reduce the dispersion of pollutants in soil, water, and air is an additional motivation (Bergaya and Lagaly, 2001). In most of these cases, identification of the microstructural and surface properties is particularly important (Yang *et al.*, 2006).

Unfortunately, most of the methods used to characterize the morphological parameters, including the adsorption of noble gases at low temperatures, mercury porosimetry, scanning electron microscopy, and many others, cannot be applied to wet porous systems. The pore systems of clays, however, particularly those of montmorillonite, can vary with changing conditions depending on the water content. In the type of thermoporometry proposed by Brun *et al.* (1977), pore space is characterized by means of freezing or melting of a liquid in the pores of the material under investigation. The change in the transition temperature is related to the pore curvature by means of the Gibbs-Thomson equation, which enables determination of the pore-size distribution. Water is the probe liquid used most often in thermoporometry, which involves the upper pore-size limit of 200 nm.

The advantage of this method is the ability to measure the internal sizes of the pores (in the case of bottle-shaped pores) in the 1.5−150 nm range. Thermoporometry seems particularly well suited to studies of wet porous samples in cases where the process of drying itself is capable of destroying the original microstructure. In addition, thermoporometry makes it possible to determine the shapes of the pores by comparing the data obtained on freezing with the data obtained on melting. In the beginning, thermoporometry was a relative method requiring calibration curves obtained from well recognized standard samples. The procedure presented by Brun *et al.* (1977) made it an absolute method, enabling the determination of pore-size distribution on the basis of theoretical relationships.

The application of thermoporometry in the investigation of the pore space of various materials has been

demonstrated by many authors: in studies by Kaneko (1994) and Rouquerol *et al.* (1994) the limitations and merits of thermoporometry were compared with those of other methods such as molecular adsorption, X-ray diffraction (XRD), and mercury porosimetry. Thermoporometry was applied by Price and Bashir (1995) to determine the location of the remaining water in polyacrylonitrile (PAN). Thermoporometry was used by Titulaer *et al.* (1995) in the investigation of silica hydrogel pores, obtaining information about ice-crystal radius, ice-pore volume, pore shape, and ice-surface area. The reliability of thermoporometry on rigid mesoporous silica with a known pore-size distribution was tested by Iza *et al.* (2000). The expected pore-radius distribution curve was obtained. Those authors also applied the technique in the characterization of the mesoporous structure of a polymeric gel swollen in an aqueous medium.

The first application of thermoporometry to a soil-water system was probably by Homshaw (1980). Based on the hysteresis between the freezing and melting temperature in the pores of two clays, he presented a theory describing the effect of pore shape on the temperatures of equilibrium freezing and melting. The analysis of the low-temperature endotherms was said by Homshaw (1980) to yield a better assessment of the pore-size distribution than the exothermic data (*i.e.* obtained on cooling). The pore-size distribution curve obtained by use of N_2-adsorption, mercury porosimetry, and Differential Scanning Calorimetry (DSC)-based thermoporometry was analyzed by Homshaw and Cambier (1980). The results confirmed that the water content of kaolin does not affect its porosity. On the basis of the DSC data the pore-size distribution curve from an individual sample could be determined. Montmorillonite was one of the materials used by Beurroies *et al.* (2004), who proposed a methodology based on thermoporometry to confirm the hysteresis phenomenon observed between the melting and solidification of a confined fluid. Thermoporometry was applied by Salles *et al.* (2008) to montmorillonite samples at a variable relative humidity (RH). By combining their results with the XRD data, a complete hydration sequence for Na-montmorillonite was proposed.

In most publications about thermoporometry, the results are presented with reservations. As a rule, the analytical results are qualitative or quasi-quantitative at best. The main reason is the occurrence of 'smearing' of the DSC peak (Höhne *et al.*, 2003) which will be discussed further below. Neffati and Rault (2001) demonstrated that "calorimetry at heating rate higher than 2 K min^{-1} gives wrong results concerning the mean pore dimension and the pore size distribution." Although this issue may not be crucial in simpler systems such as glass beads, in the case of clays, in which the pore-size distribution is less uniform, the peaks will overlap. Many authors, aware of this fact, applied low or extremely low scanning rates (*e.g.* 1 K min^{-1} by Titulaer *et al.*, 1995;

0.31 K min^{-1} by Ishikiriyama *et al.*, 1996; 0.1−0.5 K min^{-1} by Rigacci *et al.*, 1998; 0.2 K min^{-1} by Iza *et al.*, 2000; 2 K min^{-1} by Neffati and Rault, 2001; 1 K min^{-1} by Beurroies *et al.*, 2004; 2 K min^{-1} by Salles *et al.*, 2008). Unfortunately, the signal-to-noise ratio decreases dramatically with the decreasing heating rate. Another way to narrow the peaks would be to use very small samples, of the order of 1−2 mg; however, the sensitivity might become insufficient in this instance. In the present study, a method is proposed in which the broadened exothermal peak is processed by means of a stochastic deconvolution analysis. The sample masses are of the order of 10 mg and scanning rates of 5 K min^{-1} and more are used. Despite this, the result is a 'sharp' thermogram of pulse-like heat events which can be transformed easily into the pore-distribution curve.

METHODOLOGY

Identification of the starting and end points of the DSC peak

As a rule, thermoporometry is based on DSC. The term 'scanning' relates to a continuous change in the temperature of the sample and a reference in an assumed range. During the experiment, the difference in the heat flow between the sample and the reference is measured as a function of temperature, T, or time, t, (the variables being strictly connected *via* the so called scanning rate v, *i.e.* $T = vt$).

A serious problem in the analysis of the DSC signal obtained on the melting of a sample of frozen soil is the identification of the initial temperature of the summary broad peak associated with the melting of the water confined in the pores. The most common manual method is sufficient in the case of the sharp peaks corresponding to the individual phase changes, but the latent heat associated with the melting of the water in the micropores of <2 nm below −30ºC is very small and the peak in this temperature region is scarcely distinguishable from the baseline (Figure 1). Assuming a linear temperature dependence of the soil specific heat, a linear plot of the DSC signal is expected before the initiation of the ice melting. Because of the short-term noise, however, the straight line is only an approximation. The initial temperature of the peak T_{init} is identified as the temperature above which all of the signal values begin to drift away from the approximating line. In the numerical algorithm, the DSC signal between −60ºC and −30ºC is approximated by linear functions in the temperature ranges of 5 K in width. The first slope coefficient, significantly different from the others, indicates the onset of the peak. Now the linear function obtained in the previous range is the last approximation of the baseline. The temperature above which all the values of the DSC signal are smaller than the values of the approximated baseline is recognized as T_{init} (Figure 2). The final temperature, T_{final}, of the peak is
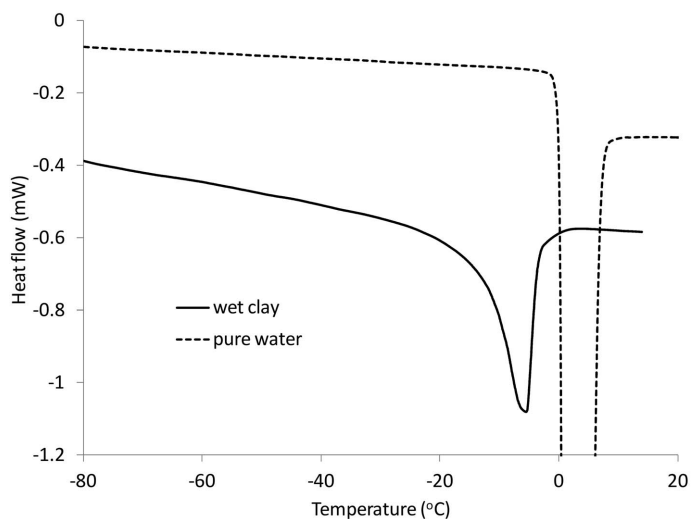
Figure 1. The DSC signals obtained on warming at a rate of 5 K min^{-1} for samples of a wet clay and pure water, both recalculated to 1 mg of water in the sample.

found in a similar manner; in this case the stepwise 5 K approximations are made between −5ºC and +20ºC.

Correction of the calorimetric peak due to the change of the baseline slope

Because of the difference between the specific heats of the solid and liquid phases of the same substance, the slopes of the approximated baselines before and after the peak are, in general, different. The common procedure, in which the endothermic peak is determined in relation to a straight line connecting the starting and the final points of the phase transition, would lead to a significant error in the case of the very broad peaks associated with the thawing of a moist soil sample. In the present method, the DSC curves obtained were corrected with reference to a sigmoid line according to an algorithm taking into account the change in the heat capacities of the sample constituents due to ice melting. The following quasi-linear equation describing a 'fluent'

sigmoid interpolation between the straight sections of the reference line before and after the interval of the phase changes was used.

Let the baseline for temperatures $<T_{init}$ be expressed by the linear equation $g(T) = a_L T + b_L$ and for temperatures $>T_{final}$ by $g(T) = a_R T + b_R$ (Figure 2). Let us assume that the notional baseline under the peak is expressed by the following quasi-linear equation:

$$\overline{g(T)} = a_S(T)\,T + b_S(T) \qquad (1)$$

where $a_S(T)$ and $b_S(T)$ are temperature-dependent coefficients varying from a_L, b_L at the temperature T_{init} to a_R, b_R at the temperature T_{final}. The degree of this transformation depends on the phase-change progress which expresses the following proportion:

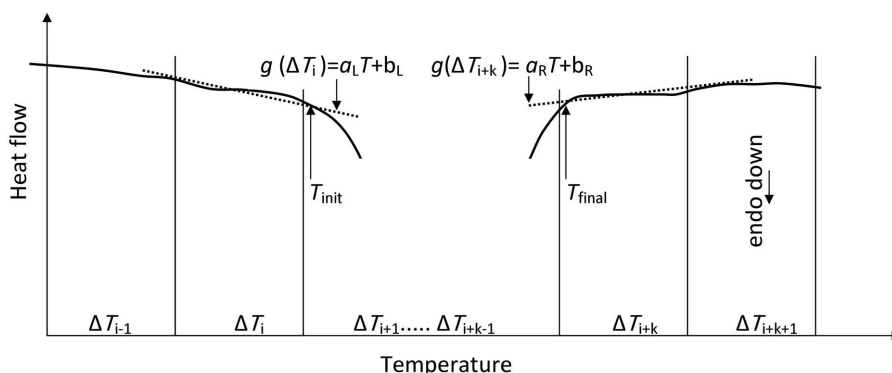$$\frac{a_L - a_R}{F} = \frac{a_L - a_S(T_i)}{\Delta F(T_i)} \qquad (2)$$

Figure 2. Schematic representation of the numerical procedure for the identification of the initial and final temperatures of the broad DSC peak obtained on melting of a wet clay sample: ΔT — temperature ranges of 5 K in width; $g(\Delta T_i)$ — the last linear approximation of the baseline before the onset of the peak; $g(\Delta T_{i+k})$ — the first approximation of the baseline after the offset of the peak.

where F is the total peak area and $\Delta F(T_i)$ is the area of the part of the peak between temperatures T_{init} and T_i, both calculated in relation to $\overline{g(T)}$. Rearranging equation 2 gives

$$a_S(T_i) = a_L(1 - \frac{\Delta F(T_i)}{F}) + a_R \frac{\Delta F(T_i)}{F} \qquad (3a)$$

and by analogy

$$b_S(T_i) = b_L(1 - \frac{\Delta F(T_i)}{F}) + b_R \frac{\Delta F(T_i)}{F} \qquad (3b)$$

The values of $a_S(T)$ and $b_S(T)$ were calculated using a recurrent method. The straight line mentioned above was the first approximation of the function $\overline{g(T)}$. In relation to it, the first approximation of the corrected peak function $\Phi(T)$ was determined as

$$\Phi(T_i) = \Phi(T_i) - \overline{g(T)} \qquad (4)$$

where $g(T)$ is the function of the calorimetric signal in the temperature interval $[T_{init}; T_{final}]$. Next, the values of $\Delta F(T_i)$ were computed as

$$\Delta F(T_i) = \int_{T_{init}}^{T_i} \Phi(T_i)dT \qquad (5)$$

Note that the same equation was used to calculate the value of F when $T_i = T_{final}$ and, of course, F corresponds to the total heat of the phase change, Q. Then the values of $\Delta F(T_i)$ and F are used, *via* equation 3, to calculate the next approximation of the notional baseline according to equation 1. The procedure was terminated when the

difference between two values of F determined successively was less than an assumed value, ε.

The results of the correction of the DSC peak by use of the linear baseline and the baseline calculated by equation 1 differ significantly from each other (Figure 3). Because the peak obtained by use of the linear baseline is significantly larger over the entire temperature range, this error is expected to lead to overestimation of the volume of the pores in a wide range of sizes. Note that the separation of the original (uncorrected) peak from the DSC signal (*i.e.* identification of the temperatures of the start and the end of melting) also requires a special numerical procedure, as described in the section on 'Identification of the starting and end points of the DSC peak'.

Deconvolution analysis of the DSC signal

Independent of the instrument construction, the heat-flux curves obtained during the DSC runs are not real thermal flux curves related to the process being investigated. Several heat-transport phenomena, such as limited thermal conductivity, the heat capacity of the instrument parts, and the time needed for heat transport (Höhne *et al.*, 2003) lead to an effect called the smearing of the experimental curve. Let us analyze a pulse-like heat event related to a phase transition of a crystalline substance. In reality the event yielded, at a strictly determined temperature T_0 (referred to as the melting or freezing point), which is recorded as a peak, $\Phi(T)$, the onset point only of which is in T_0, and the width of which is an increasing function of the scanning rate (Figure 4). More thermal impulses yield a peak which in
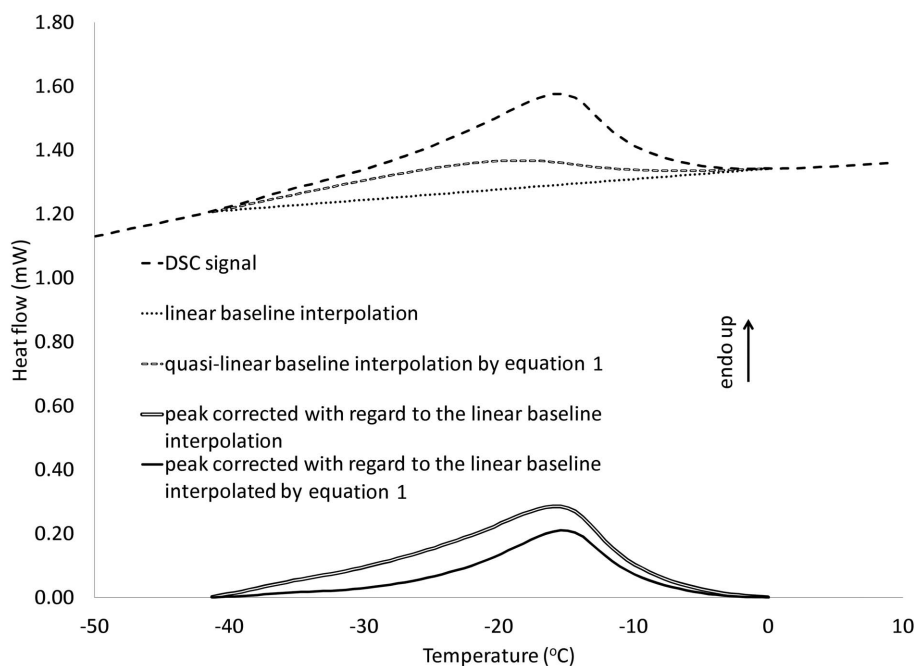

Figure 3. Raw DSC signal and the peaks corrected with regard to the linear and quasi-linear baseline interpolation.
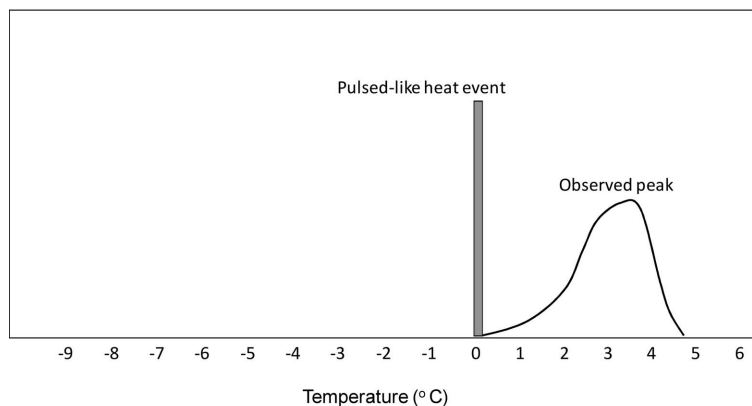
Figure 4. Response of calorimeter to a single pulse-like heat event.

fact represents the superposition of a number of peaks (Figure 5).

Normalization of the function $\Phi(T)$ (or, more formally, $\Phi(t)$) in relation to the corresponding heat, Q, and the temperature, T_0, gives an apparatus function $a(T)$ related to the construction of a given calorimeter and the ability to be estimated experimentally:

$$a(t - t_0) = \frac{\Phi(t - t_0)}{Q} \qquad (6)$$

where $\Phi(t)$ is the observed heat flux thermogram, in W, and Q is the thermal effect absorbed or yielded at time t_0 corresponding to the temperature T_0, in J.

In other words, the apparatus function is a distribution of fractions of Q observed on the DSC signal in a temperature range above (on the warming run) or below (on the cooling run) the temperature T_0. The apparatus function given by equation 6 can easily be determined experimentally from a controlled pulse-like event.

In terms of mathematics, the observed function $\Phi(t)$ is the so-called convolution product of the function of the pulse-like heat events $q(t)$ and the apparatus function $a(t)$:

$$\Phi(t) = \int\limits_{-\infty}^{\infty} a(t - t')q(t')dt' \qquad (7)$$

The problem of finding the function of the real heat flux lies in in solving equation 7 in relation to $q(t)$ when the functions $\Phi(t)$ and $a(t)$ are known. Theoretically, several methods exist to solve the problem, *e.g.* Fourier transforms, a recursion method, the ridge regression, *etc*. They all failed, however, when applied to the real DSC signal. Recovery of the original signal cannot be guaranteed in practice, as the procedure is very sensitive to noise. The results of trial computations made by the present authors using the FFT (Fast Fourier Transform), the ridge regression, and the recursive method described by Höhne *et al.* (2003) were unsatisfactory, *e.g.* yielding results with negative values (*i.e.* showing exothermic processes on melting!). The most serious disadvantage of these methods is in their abstract nature, because the calculations are made in Fourier space. As pointed out by Höhne *et al.* (2003), "under specific conditions this simulates periodicities and fluctuations which do not reflect any actual processes in the sample." These issues
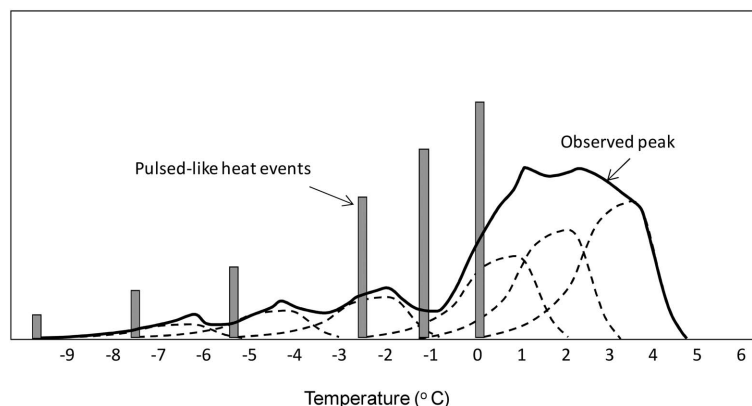

Figure 5. Response of calorimeter to several pulse-like heat events as a superposition.

do not affect the method presented based on a numerical analysis of the square deviations of the observed function $a(T)$ and the convolution of the apparatus function $a(T)$ with functions $q_i(T)$, being successive approximations of the real function $q(T)$ (note that, mathematically, equations 6 and 7 are identical both for time and temperature variables).

The observed function of heat flux $\Phi(T)$ (or the calorimetric peak) was divided into a number of finite elements of width $\Delta T_i = T_{i+1} - T_i$, each with a constant value of thermal flux $\Phi(T_i)$. The discretization applied to the apparatus function $a(T)$ also. Equation 3 in a finite differences form can be written as follows:

$$\Phi(T_i) = \sum_{i=1}^{n} \sum_{j=i}^{i+m-1} a(T_j - T_i)q(T_i)\Delta T_i \qquad (8)$$

where n is the number of elements of the observed function and m is the number of elements into which the apparatus function was divided.

The apparatus function, $a(T)$, was determined on the basis of DSC curves obtained by melting six samples of pure ice with a scanning rate of 5 K min^{-1}. For sample masses between 0.5 mg and 4.0 mg the observed shapes of the peak were very similar. The error of determination of the latent heat was <1%. One of the peaks, obtained for a sample of 1.61 mg, was chosen for the creation of the apparatus function. The main reason for this choice was the excellent result obtained for this sample: the latent heat of fusion $L = 333.32$ J/g. The observed peak was divided into fields of 1 K in width. The number of the fields, which corresponds with the value of l in equation 8, was 10. The area of each field was divided by the total area of the peak. Thus, the apparatus function obtained represents the distribution of the fractions of the total heat of fusion of ice at 0ºC,

which are observed at the wide temperature interval above as an endothermic peak (Figure 6).

A good approximation of the function $q(T_i)$ was determined by producing assumptive distributions, $q_k(T_i)$, and making their convolutions with the apparatus function $a(T_i)$ according to equation 3. The convolution product obtained, $\Phi_k(T_i)$, is a 'calculated' DSC signal (Figure 7). The following sums of square deviations were analyzed for each $\Phi_k(T_i)$:

$$D_k = \sum_{i=1}^{n} (\Phi(T_i) - \Phi_k(T_i))^2 \qquad (9)$$

The value of D_k reaches a minimum for the best approximation of $q(T_i)$.

The values of the function of heat events, $q(T_i)$, obtained, multiplied by the widths of the temperature intervals, ΔT_i, express a distribution of the conventional heat impulses attributed to the temperature intervals. The temperature of the last non-zero impulse is the temperature of the end of melting, T_0, or the melting point, with an accuracy equal to the length of the temperature interval, ΔT_i.

During calculations, the total heat, Q, was divided into elementary 'bricks'. Initially, the value of each brick was 1/35 of Q. In subsequent stages, the value of an individual brick was divided by 2, hence the total number of the bricks increased according to the geometric progression: 35, 70, 140, 280, and 560. At each stage, the bricks were distributed at possible temperature positions, the number of which was 40 (the computations were carried out in the range −40ºC to 0ºC because heat events were not expected above 0ºC). In terms of combinatorics, the distributions are permutations with repetitions of length k (the number of bricks) from the n-elements set of temperatures. For $k = 35$, $40^{35} \approx 1.2E56$ arrangements

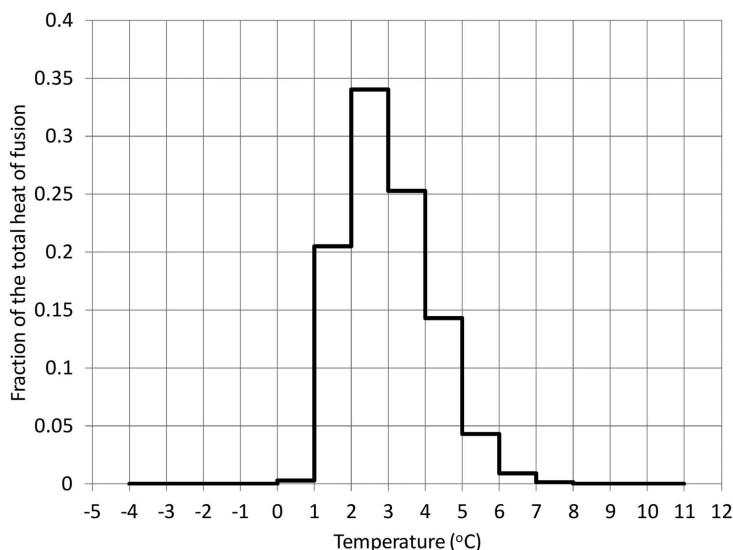Figure 6. The apparatus function obtained from the melting peak of a sample of pure water at the scanning rate of 5 K min^{-1}
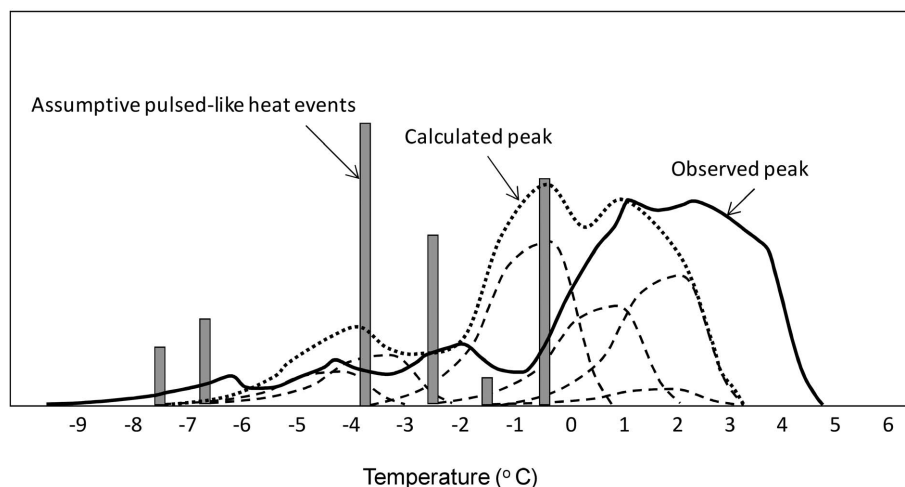
Figure 7. The observed DSC signal *vs*. the DSC signal calculated by convolution of an assumptive distribution of the pulse-like heat events with the apparatus function.

were obtained; hence an ultrafast computer would need billions of years to examine all of the distributions. For this reason, only more probable arrangements were examined, identified by use of subtle procedures (*e.g.* an arrangement at which 10/35 of Q goes into -38°C can be eliminated in advance). The term 'stochastic' used in the name of the method, therefore, is inappropriate in the strict sense and refers only to the fact that, to an extent, searching for the best arrangement is carried out blindly.

According to equation 8, the convolution of $q_k(T_i)$ with $a(T_i)$ was made and fitting was checked out by use of equation 9. A pass to another stage occurred after finding such a distribution of the fractions that gave a minimum of D_k, *i.e.* when the calculated and observed DSC signals are as close to each other as possible (Figure 8).

Obtaining pore-size distribution from the pulse-like heat event distribution

Relating the melting temperature to the pore radius. The pulse-like heat event distribution $q(T)$ can be used in the analysis of the pore space according to the following procedure.

For the soil-water system, the main thermoporometry equation can be written as follows (Fabbri *et al*., 2006):

$$T_f = g^{-1}\left(\frac{2g}{r_p - e}\right) \qquad (10)$$

$$T_m = g^{-1}\left(\frac{g}{r_p - e}\right) \qquad (11)$$

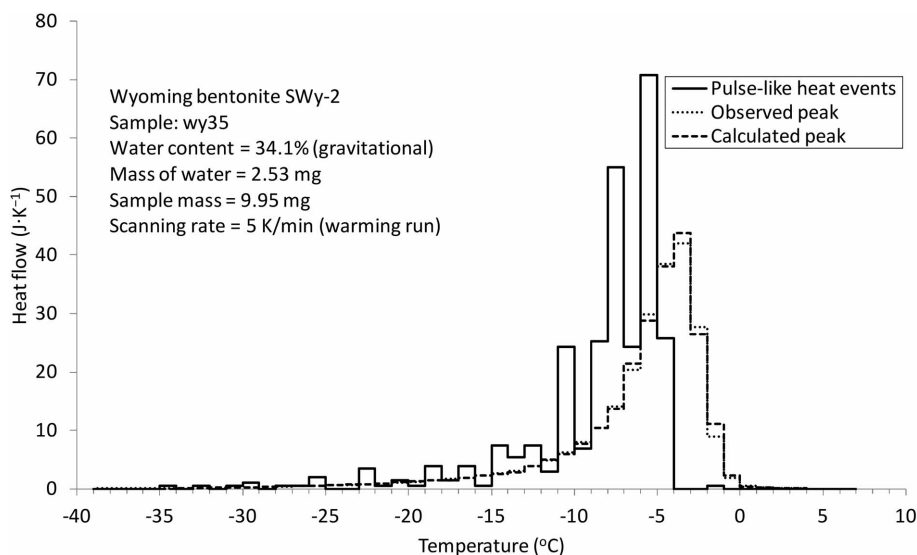Figure 8. Functions of pulse-like heat events $q(T)$, the observed calorimetric DSC signal, $\Phi(T)$, and the best-fitted DSC signal calculated by convolution of $q(T)$ and $\Phi(T)$ (all separated into 1° intervals).

where T_f and T_m are the freezing and melting temperatures, respectively; r_p is the corresponding pore radius for an ice crystal in the cylindrical pore, in equilibrium with the liquid water in the adjacent pores; γ is the water/ice interface energy; e is the thickness of the layer of the adsorbed water not undergoing phase changes; and g^{-1} is a function inverse to a state function given by Fabbri *et al.* (2006) in the following form:

$$g(T) = S_f(T_0 - T) + C_f(T - T_0 + T \ln\left(\frac{T_0}{T}\right)) \quad (12)$$

where S_f is the entropy of fusion per unit of the ice-crystal volume, C_f is the heat capacity difference between water and ice per unit of ice crystal volume and T_0 is the water freezing point at normal conditions.

According to Brun *et al.* (1977), $S_f \approx 1.2$ MPa/K and $C_f \approx 2.1$ MPa/K, and the temperature T_0 is expressed by the Raoult law as:

$$T_0 = T_{00} - Km_0 \quad (13)$$

where T_{00} is the solidification temperature of pure water in bulk at atmospheric pressure (= 273.15 K), m_0 is the initial molality (~1 mol/kg for a cement paste >90 days old; Fabbri *et al*., 2006), and K is the cryoscopic Raoult coefficient, dependent on the solvent and regardless of the solute. In the case of the water solvent, $K = 1.86$ (Zuber and Marchand, 2000 after Fabbri *et al.*, 2006).

For the water/ice interface energy in equations 6 and 7, Fabbri *et al.* (2006) proposed the following simplified equation:

$$\gamma = 36 + 0.25(T - T_{00}) \quad (14)$$

in which γ is expressed in N/m.

Determining the thickness of the layer of adsorbed water. In order to determine the value of e, the following procedure was applied. By use of the pulse-like heat events, distribution $q(T_i)$, the unfrozen water content function, $w_u(T_i)$, can be determined as follows:

$$w_u(T_i) = w - \sum_{j=i}^{n} \frac{100q(T_j)\Delta T_j}{L(T_j)m_s} \quad (15)$$

where $w_u(T_i)$ is the unfrozen water content at a temperature T_i as a percentage of the dry mass, w is the water content expressed as a percentage of the dry mass, $L(T_j)$ is the latent heat of fusion of ice at the temperature T_j, and m_s is the mass of dry soil in the sample, in g.

Equation 15 allows us to determine the so-called 'unfreezable' water content, w_{unf}, *i.e.* the unfrozen water content at the temperature at the beginning of the observable process of melting (in this case, the summation involves all the pulse-like heat events found and therefore w_{unf} is the difference between the total water content, w, and the sum of the elementary 'portions' of ice melted during the melting process). The volume of the unfreezable water can now be determined as:

$$V_{unf} = (w_{unf}m_s)/(100\rho_{un}) = Sm_s e \quad (16)$$

Under the assumption that the unfreezable water corresponds to the adsorbed water, equation 16 allows us to determine the thickness of the layer of the adsorbed water:

$$e = w_{un}/(100\rho_{un}S) \quad (17)$$

where ρ_{un} is the density of the unfreezable water and S is the total surface area of soil.

The values of S, obtained from the Water Sorption Test (WST) proposed by Stepkowska *et al.* (2004), are recommended for use in the calculations. The external specific surface is obtained as the product of the water content after sorption at RH = 0.50 (g H_2O/g dry clay) and a constant ratio equal to 585 m^2/g H_2O. Then, the total surface area is calculated from the external surface area. The technique gives trustworthy information regarding the specific surface and the particle thickness of smectites, fully comparable with other methods, including XRD (Stepkowska *et al.*, 2004). In the context of thermoporometry, determination of the specific surface on the basis of the water-sorption data appears reasonable, in contrast to the techniques using sorption of other non-polar (N_2, Ar) or polar molecules (glycerol, ethylene glycol, methylene blue).

A value of 1.27 g/cm^3 can be used for the density, ρ_{un}. According to Stepkowska *et al.* (2004), such a value applies to a bimolecular layer of water adsorbed on clays. Upon comparison of the data in Tables 1 and 2 it is apparent that the quantity of the unfreezable water corresponds approximately to the water adsorbed at the relative humidity RH = 0.95. In such conditions, however, only a bimolecular layer is formed (Stepkowska *et al.*, 2004).

Calculating the quantity of ice melting in a given temperature range. Equations 10−16 make it possible to relate the temperatures of phase changes to the pore radius. The value of a pulse-like heat event associated with a given temperature can also be used to calculate the quantity of water undergoing phase changes in the corresponding temperature range, ΔT_i:

$$m_w(\Delta T_i) = \frac{q(\Delta T_i)}{L(T_i)} \quad (18)$$

where $m_w(\Delta T_i)$ is the amount of water undergoing a phase change when the temperature changes by ΔT_i, $q(\Delta T_i)$ is the thermal effect associated with the temperature change, ΔT_i, and $L(\Delta T_i)$ is an average value of the latent heat of fusion in the temperature range, ΔT_i. In the calculations presented, the lengths of the temperature intervals, ΔT_i, were equal to 1 K.

Equation 18 can then be used to determine the change of pore-ice volume on melting when the temperature rises by ΔT_i:

Table 1. Selected properties of the clays.

Symbol	Major exch. cations	Clay fraction (%)		Consistency limits (%)		CEC (meq/100 g dry soil)	Water content after sorption at RH = 0.50	Water content after sorption at RH = 0.95	Specific surface area (m²/g) Water Sorption Test (WST)/ EGME and BET method	
		Hydro-meter	Laser diffraction	LL	PL				Total	External
STx-1b	Ca^{2+}	73.3	14.6	142	44	84.4	16.90	28.76	593.22/ 534	98.87/ 74
SWy−2	Na^+/Ca^{2+}	60.4	45.4	519	35	76.4	9.47	22.68	332.52/ 637	55.42/ 29*

* 22.7 m²/g according to Dogan *et al.* (2006).
LL: liquid limit; PL: plastic limit

$$V_{ice}(\Delta T_i) = \frac{q(\Delta T_i)}{L(T_i)\rho_{ice}} \qquad (19)$$

which, *via* equations 11, 12, and 17, can be attributed to the volume of pores of a given radius r_p.

The temperature dependence of the latent heat. Equations 15, 18, and 19 require the temperature dependence of the latent heat of ice melting, $L(T)$. This point still causes controversy. According to Efimov (1986), any strictly theoretical approach cannot be fully successful due to the lack of appropriate data. Instead, approximate or empirical equations are used. The matter becomes more complicated when the adsorbed or confined water is in question. The free energy of the bound water falls between the energies of liquid water and ice (Turov and Leboda, 1999) and, consequently, the latent heat of fusion of water adsorbed in a monolayer is about half of the analogous value for water in bulk (Efimov, 1986). The following formula, obtained experimentally for water freezing on silica gels, was presented by Horiguchi (1985):

$$L(T) = 7.3T + 334 \qquad (20)$$

where $L(T)$ is the latent heat of fusion of ice at temperature T in J/g and T is the temperature in ºC.

Similar values are given by the following quadratic equation (Price and Bashir, 1995):

$$L(T) = 0.0556T^2 + 7.42T + 332 \qquad (20)$$

The differences increase with decreasing temperature (Figure 9), being insignificant above −10ºC and increasing significantly below −30ºC. The fact that Horiguchi's formula yields zero value of latent heat at ~−46ºC seems slightly confusing. A formula for super-cooled water based on the differences in the densities of liquid water and ice, presented by Nevzorov (2006), however, predicts the vanishing of the latent heat at −39ºC. According to Nevzorov (2006), such behavior may be attributed to the state at the temperature of homogenous nucleation at which the internal energies of liquid water and ice−I become equal. Some individual values given by Fung and Burke (1996) speak in favor of Horiguchi's formula. Data presented by Bogdan and Kulmala (1997), however, show a dependency on the relative humidity at which the adsorption took place (a quantity relating to the number of conventional mono-layers of the adsorbed water). Apparently, when talking about the temperature dependency of the latent heat we actually talk about the relationship between the state of the adsorbed water, the temperature of its phase change, and the latent heat related to this process.

Note that the differences for temperatures below −10ºC (Figure 9) seem insignificant, because the intensity of the phase changes in soil-water systems decreases with temperature and, *ipso facto*, the influence

Table 2. Measures of dispersion of the unfreezable water content calculated by use of three different functions describing the temperature dependence of the latent heat, L.

w (%)	SWy-2			w (%)	STx-1b		
		w_{unf} (%)				w_{unf} (%)	
	L = const.	$L(T)$ by eq. 20	$L(T)$ by eq. 21		L = const.	$L(T)$ by eq. 20	$L(T)$ by eq. 21
34.1	22.90	19.78	20.10	41.83	25.91	20.72	21.52
85.82	24.81	19.73	19.46	50.7	26.72	21.00	21.78
86.38	22.08	17.01	16.71	63.74	27.77	21.72	22.44
88.41	22.18	17.19	16.91	64.86	27.25	21.85	22.37
98.11	22.23	17.00	16.76	70.06	28.18	22.62	23.06
117.51	21.54	15.71	15.35	70.08	30.32	25.18	25.36
				70.51	26.09	20.58	20.96
				81.72	26.51	20.26	21.00
Valid N	6	6	6	Valid N	8	8	8
Mean	22.62	17.74	17.55	Mean	27.34	21.74	22.31
Minimum	21.54	15.71	15.35	Minimum	25.91	20.26	20.96
Maximum	24.81	19.78	20.10	Maximum	30.32	25.18	25.36
Variance	1.34	2.73	3.35	Variance	2.07	2.54	2.04
Std. dev.	1.16	1.65	1.83	Std. dev.	1.44	1.59	1.43
Coef. var.	5.11	9.31	10.42	Coef. var.	5.26	7.32	6.41
Thickness, e (nm)	0.536	0.420	0.416	Thickness, e (nm)	0.363	0.289	0.296

of varying values of $L(T_i)$ also diminishes at lower temperatures. Assuming a temperature-independent, constant value of L, however, (as commonly done by many authors) may lead to an underestimation of the quantity of ice melting at a given temperature. More detailed discussion in relation to the present results is given below.

MATERIALS AND EXPERIMENTAL PROCEDURE

Natural montmorillonites from Texas (STx-1b) and Wyoming (SWy-2) were used (Table 1). The clays were obtained from the Source Clays Repository of The Clay Minerals Society, Chantilly, Virginia, USA. The intention was to study clay−water systems as naturally as possible. The clays were not processed other than to add deionized water to form a paste with a consistency close to the liquid limit. A sample of the paste was placed in an aluminum calorimetric vessel and smeared uniformly over the bottom. The vessels were not encapsulated and the pastes were allowed to air dry to different extents. The approximate temporary water content was controlled by weighing and when the water content reached a required value, the vessel was sealed hermetically.
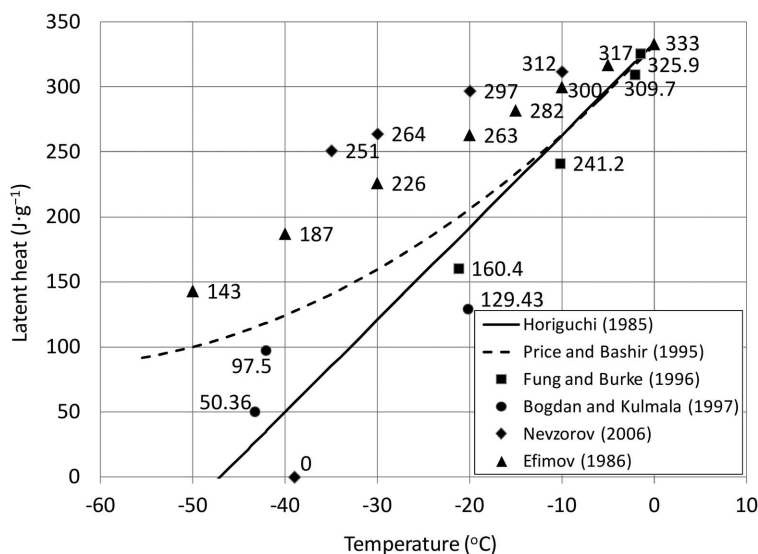

Figure 9. Temperature dependences of the specific enthalpy (latent heat) of water freezing.

Then the mass was determined accurately and the calorimetric experiment was carried out. The samples were cooled with the scanning rate of 2.5 K min^{-1} to -90°C and then warmed at the scanning rate 5 K min^{-1} to $+20$°C. The DSC Q200 differential scanning calorimeter with a refrigerated cooling system RCS90, manufactured by TA Instruments (New Castle, Delaware, USA), was used in the experiments. The RCS90 enables an operating range of -90°C to 550°C.

After the experiment, the vessel was weighed again to control any unexpected loss of hermeticity. Next, pinholes were punched in the sample covers and the total water content was determined by drying to a constant mass at 110°C.

Such sample preparation differs from the widely used method in which different water contents are obtained at different relative humidities. Although the latter is thought to allow for obtaining water contents more strictly defined in terms of clay mineralogy, the matter is not so simple. On the one hand, the hydration process is very complicated (Salles *et al.*, 2008). The current state of knowledge does not allow us to link thermoporometric data to strict states of a porous network at individual stages of hydration; in contrast, thermoporometry can be used to extend our understanding of this issue. On the other hand, however, the water in natural soils never occurs at constant humidities and, moreover, natural water contents are usually greater than the water contents obtained in the laboratory at humidities $\leqslant 0.95$. The hydration in this case proceeded irregularly, by the repeated supply with liquid water and the subsequent uncontrolled evaporation. The results presented attempt to show to which extent the pore-size distribution remains a function of the water content in such quasi-dynamic conditions.

Only results obtained during the warming DSC run were analyzed and consequently the non-equilibrium phenomena associated with supercooling were avoided. The procedure proposed by many authors (*e.g.* Titulaer *et al.*, 1995; Torralvo *et al.*, 1998; Iza *et al.*, 2000; Beurroies *et al.*, 2004) in which an initially frozen sample is warmed to a temperature close to zero and then the experiment on cooling is carried out appears to be unsuitable at higher water contents. In this case, the freezing begins at close to zero and the baseline cannot be determined reasonably.

In addition to thermoporometry, the pore network of the bentonites was investigated using two alternative techniques: (1) N$_2$ adsorption at 77 K with subsequent analysis by use of the model proposed by Barrett, Joyner, and Halenda (BJH) — data from the adsorption curve were used; and (2) mercury intrusion porosimetry (MIP) — data from the intrusion curve were used.

In each instance, standard procedures were applied and the data were processed by means of the software provided by the equipment manufacturer (Micromeritics ASAP 2020 and Micromeritics AutoPore IV 9500, respectively).

Because both of the methods involve the complete drying of the samples prior to investigation, however, the results cannot be fully comparable. Moreover, both of these techniques are based on an unrealistic assumption of a cylindrical pore shape, whereas wedge-shaped pores are recognized by imaging techniques (Velde *et al.*, 1996).

RESULTS AND DISCUSSION

The unfreezable water content vs. the temperature dependence of the latent heat

As shown in the section on 'Pore-size distributions' the unfreezable water content, w_{unf}, , *i.e.* the amount of water not undergoing phase changes, can be determined *via* equation 16. In turn, w_{unf} can be used to calculate the thickness of the adsorbed layer on the pore walls, according to equation 17. Unfortunately, a function describing the temperature dependence of the heat of melting, $L(T)$, is still unavailable. Attempts were made to assess the effect of the $L(T)$ relationship on the unfreezable water content, w_{unf}, making calculations according to equation 16 using three variants: (1) with constant $L = 333.62$ J/g; (2) with $L(T)$ according to equation 20; and (3) with $L(T)$ according to equation 21. Under the assumption that the unfreezable water content, w_{unf}, is independent of the total water content, less dispersion of the results is expected with 'more proper' applied relationships. The results are thought-provoking (Table 2). The measures of dispersion, *i.e.* the standard deviation and the coefficient of variation, do not definitively indicate the temperature-dependent relationships to be more realistic than the constant function. This is particularly apparent in SWy-2, where the dispersion of w_{unf} is least at constant L. The temperature dependence given by equation 20 yields less dispersion than does equation 21. For STx-1b, in contrast, the results are somewhat similar for $L = $ const and L given by equation 21, and they are the worst for L according to equation 20. The distribution of pulse-like heat events in these two experimental soils are significantly different, reflecting the differences in the pore-size distributions. Strikingly, the results obtained for constant L are almost equal to the water contents adsorbed at the relative humidity RH $= 0.95$ (cf. Table 1). According to Stepkowska *et al.* (2004), such water content corresponds to the maximum amount of water adsorbed in a clay–water system.

Worthy of note are that the thicknesses of the adsorbed layer, e, obtained for the temperature-dependent values of L seem the most realistic (Table 2). Assuming the thickness of the monolayer is equal to the diameter of the water molecule (~0.28 nm), the results indicate that the unfreezable water relates almost exactly to a monolayer on STx-1b and a double layer on SWy-2. As indicated by Optiz *et al.* (2007), "It is important to note that a water double layer is thinner than two
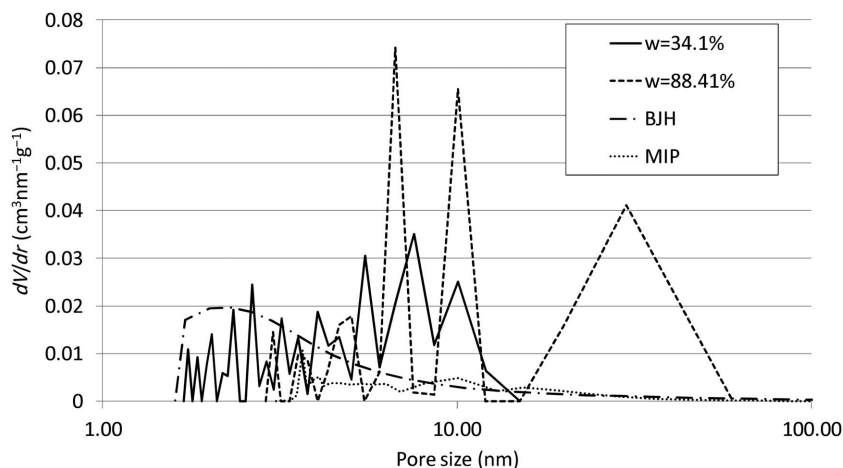
Figure 10. The differential pore-size distribution (PSD) curves of two samples of SWy-2 with two different water contents obtained by thermoporometry compared to the results obtained by BJH and MIP.

monolayers of free water molecules." The difference is probably due to the different exchangeable cation composition in these two bentonites.

Nonetheless, either the proposed relationships for the temperature dependency of the latent heat are too radical, *i.e.* the variation of the latent heat of ice fusion in soils is significantly less, or the unfreezable water content, w_{unf}, for whatever reason, depends on the total water content. This issue deserves further investigation.

The pore-size distributions

In view of the different pore-size distribution curves obtained (Figures 10, 11), the method of pore-network investigation presented seems trustworthy. Firstly, the curves of the pore-size distribution obtained are exceptionally sharp. Secondly, the results are repeatable, which is apparent from comparison of the different pore-

distribution curves obtained for samples of the same clay with similar water contents (Figures 12, 13).

In the distribution of the pulse-like heat events obtained, distributions with repeated zero values predominated. Apparently, this reflects a discontinuity of the pore-size distributions. Note that the resolution in the variant of thermoporometry presented is limited to 1/560th of the total heat, Q, corresponding to the warming of a sample, which means that the zero values can be attributed to such a temperature range, ΔT, in which the real thermal event was less than the above-mentioned fraction of the total heat. This reservation does not change the fact that the results give strong evidence of the discontinuity of the PSD. If the real distribution was continuous, as suggested by the BJH data, the computer program would consider a continuous distribution (with an accuracy of ΔT) as the most
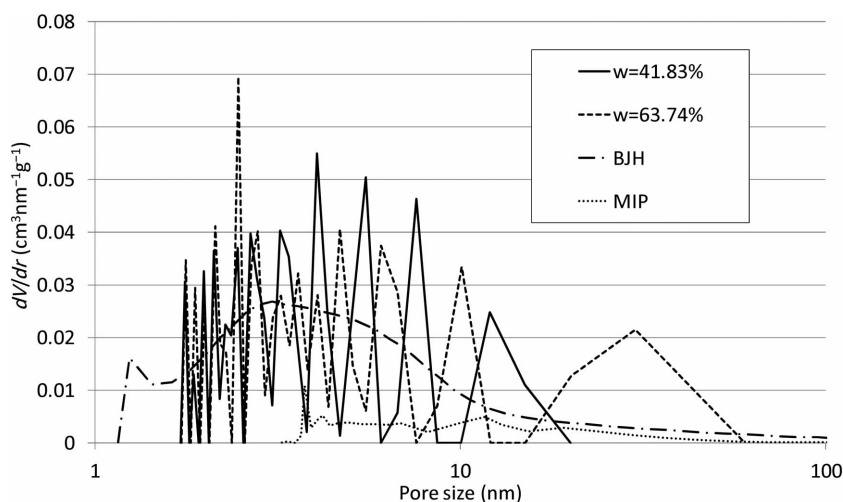

Figure 11. The differential pore-size distribution (PSD) curves of two samples of STx-1b with two different water contents obtained by thermoporometry compared to the results obtained by BJH and MIP.
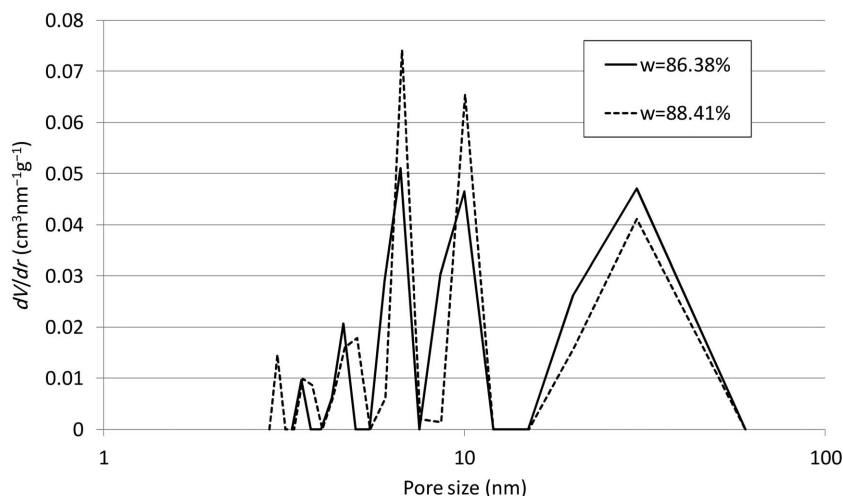
Figure 12. The differential pore-size distribution (PSD) curves of two samples of SWy-2 with two almost identical water contents.

probable. On the other hand, the continuity of the PSD suggested by the BJH and the MIP techniques may result from the not fully realistic assumption of cylindrical pore morphology, as mentioned above.

The MIP method gives evidence for the peaks lining up close to the peaks obtained by the TMP (thermo-porometry) method, principally in the samples with smaller water contents, especially for the peak at ~10 nm observed both in SWy-2 and STx-1b. The less than impressive lower limit of the pore size (3 nm), however, remains the greatest disadvantage of the MIP method. Additionally, the method is destructive and the samples must be reprocessed after the experiment.

The PSD curve obtained by BJH method is an envelope of the sharp peaks obtained by TMP (Figures 10, 11). Because the BJH method is considered a kind of standard test procedure for the measurement of the mesopore-size distribution, this fact testifies to the reliability of the TMP results. In view of the results,

however, the BJH method appears to be somewhat inappropriate for exploring systems as complex as clays and clay minerals. Its major advantage consists of the lower limit of the pore size possible, but, as seen from the PSD curves for the Wyoming montmorillonite (Figure 10), the lower limit by TMP may not differ from that of BJH in the cases of samples with small water contents investigated at high scanning rates, which increases the sensitivity of the DSC method. On the other hand, at scanning rates as high as in the present study (5 K min^{-1}), deconvolution of the DSC signal seems essential. Information on the pores in SWy-2 equal to and greater than 1.74 nm is given in Figure 10. Strikingly, in the sample of STx-1b with a water content of 41.83% (Figure 11), the presence of pores equal to 1.76 nm was indicated. These two samples represent clays in a solid consistency, below the plastic limit, so they are fully comparable. The BJH method shows the existence of a significant fraction of micropores with
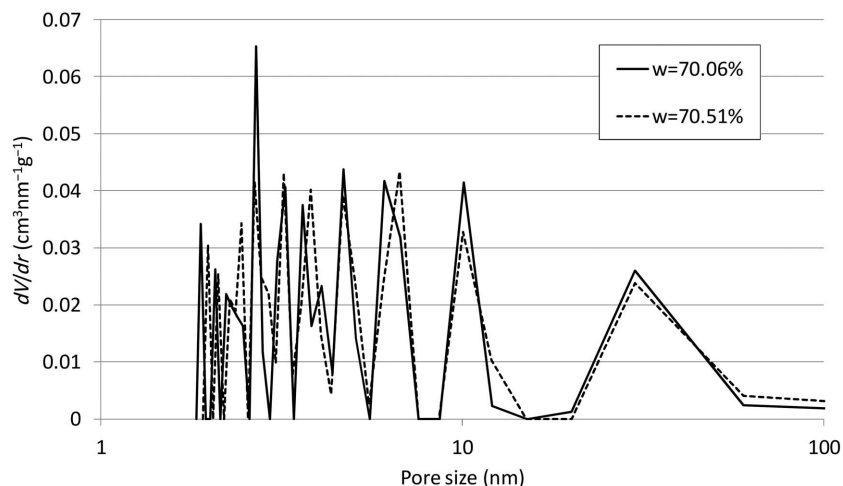
Figure 13. The differential pore-size distribution (PSD) curves of two samples of STx-1b with two almost identical water contents.

dimensions of 1.24 nm, however, the manifestation of which is the sharp peak on the left side of the PSD curve. Taking into account the unfreezable water content in the driest sample of STx-1b, such a pore dimension would correspond to the temperature of melting equal to −66ºC. Signals at such low temperatures were not observed on warming from −90ºC; theoretically, such observations would be possible for large samples warmed up at high scanning rates (10 K min^{-1} and above). A reasonable and comprehensive theory of solidification of the water confined in such small micropores is lacking, however (Alba-Simionesco *et al.* 2006; Swenson *et al.*, 2013) and we cannot exclude the possibility that this water never freezes. On the other hand, as shown by Ravikovitch *et al.* (1997), the BJH method can overestimate the results. If this is the case, just the data on the smallest mesopores obtained by thermoporometry would be more realistic in the case of the clays under investigation.

The effect of the water content

For both of the clays (Figures 10, 11), the peak maxima depend on the total water content, shifting leftward with decreasing *w*. Almost every peak observed at the higher water content has, at the lower water content, its counterpart at a position corresponding to a smaller pore dimension. The amount of this shift appears to depend on the pore size (Figure 14), *i.e.* the larger the initial pore sizes are, the greater is the corresponding decrease. The phenomena observed undoubtedly reflect the shrinkage process due to the drying that took place in all the samples prior to the experiments (*cf.* the section on 'Pore-size distributions').

A more general insight into the variation of the pore distribution during the drying process can be provided by studying the total volume of pores *vs.* the total water content (Figures 15, 16) for four classes of pores: (1) all the pores in a sample; (2) macro- and mesopores >10 nm; (3) mesopores between 3 and 10 nm; and (4) micropores <3 nm (for the purpose of this paper, the classical boundary value equal to 2 nm has been extended).

A comparison of the plots (Figures 15, 16) reveals the following observations: both the total pore volume V_{total} and the volume of pores >10 nm $V_{>10}$ are linear functions of the water content; at the corresponding water contents, the values of V_{total} and $V_{>10}$ are significantly greater in SWy-2 than in STx-1b and the difference decreases with decreasing water content; in STx-1b, the linear trend seems to break at large water contents (>80%), and, for both clays, the dependency of the volume of pores between 3 and 10 nm, V_{3-10}, and the volume of pores <3 nm, $V_{<3}$, on the water content appears insignificant.

The following linear function was analyzed:

$$V_p = aw + b \tag{22}$$

where V_p is a pore volume, the total volume, or one of the ranges mentioned above, in cm^3/g, and *w* is the gravimetric water content.

The estimates of the parameters *a* and *b* have been found together with the corresponding significance levels, *p*, the correlation coefficients (Table 3). The results confirm the initial qualitative observations. The correlations with the water content are strong and significant in the cases of V_{total} and $V_{>100}$. Both of the parameters in equation 22 are statistically significant. Notice that such a linear relationship is not trivial in view of equation 19, in which the volume of ice melting in the individual temperature ranges (*i.e.* corresponding to a pore dimension) is a function of the non-linear distribution of the pulse-like heat events and the
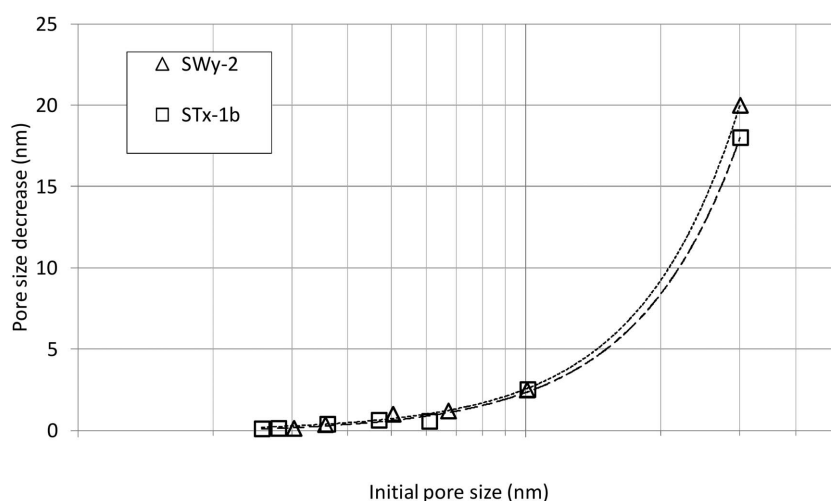

Figure 14. Pore-size decrease due to shrinkage *vs.* initial pore size observed for two samples with significantly different water contents (described in Figures 10 and 11); binomial approximations added for better readability.
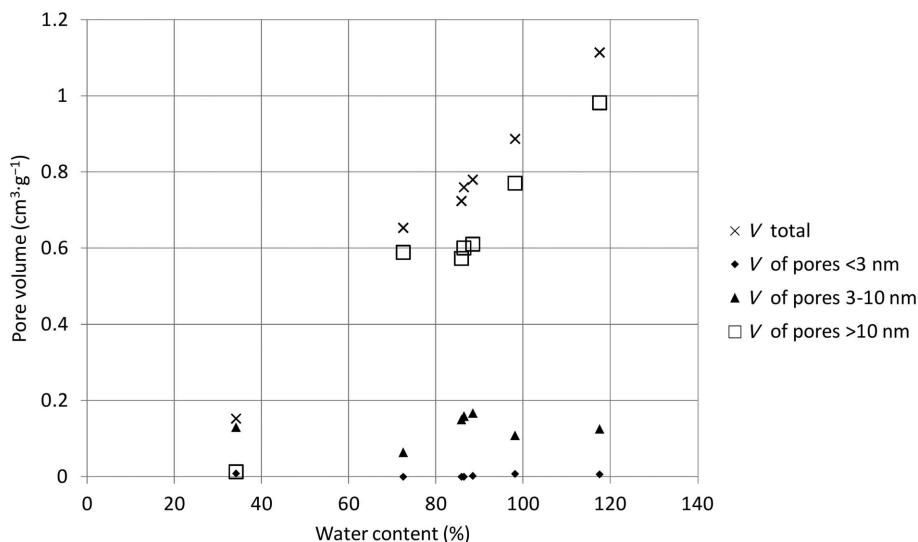
Figure 15. The total pore volume of SWy-2 and the volumes associated with three pore-size ranges *vs.* the water content.

temperature-dependent heat of fusion, L. The negative values of b have no physical sense. They would represent the pore volume at zero water content, but, of course, equation 22 is not valid below a water content corresponding to the unfreezable water content, *i.e.* at water contents corresponding to adsorbed water not undergoing phase changes. The values of unfreezable water content in both clays are much lower than the lowest water contents under investigation (Table 2). Strictly speaking, such a water content below which the pore volumes remain independent of the water content is expected to be greater than the unfreezable water content and corresponds to the so-called 'shrinkage limit'. It may be approximately related to the maximum pore volume determined by use of the N_2 sorption technique and the BJH method. The limiting water contents

calculated from equation 22 for the pore volumes, V_{BJH}, are 27.6% and 42.7%, for SWy-2 and STx-1b, respectively. Consistent with expectations, they are considerably greater than the corresponding values of the unfreezable water content. These values appear reasonable and do not contradict other results obtained.

CONCLUSIONS

(1) The application of the stochastic convolution method to the analysis of the DSC signal enables the determination of the distribution of the pulse-like heat events $q(T)$ absorbed by the frozen soil sample during the warming DSC run. It is based on searching for a distribution of 'heat events' in relation to the tempera-ture, which, convolved with the apparatus function, $a(T)$,
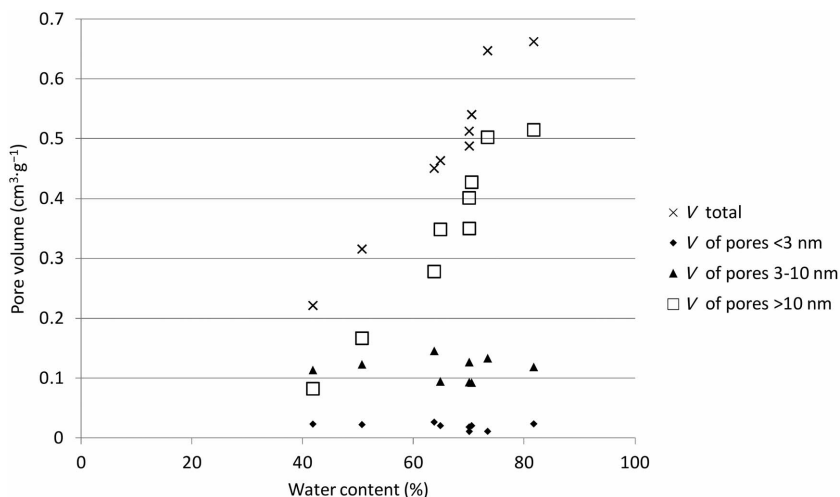

Figure 16. The total pore volume of STx-1b and the volumes associated with three pore-size ranges *vs.* the water content.

Table 3. Fitting parameters of the function by equation 22 (the values significant at the 0.05 level are shown in bold).

		— V_{total} —		— $V_{>100}$ —		— V_{30-100} —		— $V_{<30}$ —	
		Estimate	p	Estimate	p	Estimate	p	Estimate	p
	a	**0.01134**	0.00000	**0.01123**	0.00009	0.00014	0.82253	−0.00002	0.80133
SWy-2	b	**−0.22011**	0.00210	**−0.34377**	0.01015	0.11750	0.07612	0.00496	0.42609
	R	0.99632	0.98118	0.10511	0.11784				
	a	**0.01139**	0.00001	**0.01162**	0.00002	−0.00007	0.91550	−0.00015	0.36251
STx-1b	b	**−0.26477**	0.00588	**−0.41658**	0.00074	**0.12003**	0.01840	**0.02975**	0.02499
	R	0.97280	0.96976	0.04154	0.34547				

gives a minimal deviation from the observed heat flux function, $h(T)$. This algorithm ensures stability, because a testing procedure is somehow involved in it.

(2) The version of thermoporometry presented, based on the pulse-like heat events, $q(T)$, is characterized by a greater resolution than achieved by classical thermoporometry using the unprocessed DSC signal. The method also enables adjustment of fast scanning rates of the order of 5 K min^{-1} and above, resulting in increasing sensitivity, allowing measurement of micropores ~1.7 nm in diameter. The disadvantages of the method are as follows: (a) the calculations are extremely time consuming, taking 3−14 days depending on the distribution of the pulse-like heat events; (b) the need to discretize the 1 K intervals leads to the decrease in resolution (which, regardless, remains significantly better than in the classical variant of thermoporometry); (c) the lack of information about the regions in which the freezing does not occur, i.e. the interlayer space of montmorillonite; (d) a problematic value of the results for pores larger than 60 nm (ice crystals contained in such pores melt in the temperature range between −1ºC and 0ºC; hence, due to the temperature discretization, they are not detectable).

(3) The method allows us to take into account the temperature dependence of the latent heat, L; however, in view of the results, the question of the form of such a relationship remains open. Assuming a constant value of L led to neither more controversial nor more dispersed results.

(4) The distributions of the pulse-like heat events obtained testify to a considerable discontinuity of the pore-size distributions in clay−water systems.

(5) The method seems particularly useful in order to study the effect of the water content on the swelling clay microstructure. The results obtained on samples with large water contents and subjected to free drying allow us to study the evolution of the pore network as a function of the water content in the source clays SWy-2 and STx-1b. The shrinkage applies primarily to mesopores of >10 nm, the volume of which is almost a linear function of the water content. Such a result would be explained by the existence of a significant fraction of pores of <10 nm, the sizes of which are not changed with

a decrease in the water content above a boundary value. This excess water is accumulated only in large interparticular mesopores of >10 nm, the structure of which allow unlimited expansion. The evident repeatability of results obtained for different samples of the same water content prove that the process of desiccation occurs according to a strict rule, regardless of the unstable drying conditions.

ACKNOWLEDGMENTS

REFERENCES

Alba-Simionesco, C., Coasne, B., Dosseh, G., Dudziak, G., Gubbins, K.E., Radhakrishnan, R., and Sliwinska-Bartkowiak, M. (2006) Effects of confinement on freezing and melting. *Journal of Physics: Condensed Matter*, **18**, R15−R68.

Bergaya, F. and Lagaly, G. (2001) Surface modification of clay minerals. *Applied Clay Science*, **19**, 1−30.

Beurroies, I., Denoyel, R., Llewellyn, P., and Rouquerol, J. (2004) A comparison between melting-solidification and capillary condensation hysteresis in mesoporous materials: application to the interpretation of thermoporometry data. *Thermochimica Acta*, **421**, 11−18.

Bogdan, A. and Kulmala, M. (1997) DSC study of the freezing and thawing behavior of pure water and binary H_2O/HNO_3 and H_2O/HCl systems adsorbed by pyrogenic silica: implications for the atmosphere. *Journal of Aerosol Science*, **28**, Suppl. 1, S507−S508.

Brun, M., Lallemand, A., Quinson, J-F., and Eyraud, Ch. (1977) A new method for the simultaneous determination of the size and the shape of pores: the thermoporometry. *Thermochimica Acta*, **21**, 59−88.

Carrado, K.A. and Komadel, P. (2009) Acid activation of bentonites and polymer-clay nanocomposites. *Elements*, **5**, 111−116.

Dogan, A.U., Dogan, M, Onal, M., Sarikaya, Y., Aburub, A., and Wurster, D.E. (2006) Baseline studies of the Clay Minerals Society Source Clays: Specific Surface Area by Brunauer Emmett Teller (BET) method. *Clays and Clay Minerals*, **54**, 62−66.

Dogan, M., Dogan, A.U., Yesilyurt, F.I., Alaygut, D., Buckner, I., and Wurster, D.E. (2007) Baseline studies of the Clay Minerals Society Special Clays: Specific Surface Area by Brunauer Emmett Teller (BET) method. *Clays and Clay*

Minerals, **55**, 534−541.

Efimov, S.S. (1986) Temperature dependence of the heat of crystallization of water. *Journal of Engineering Physics and Thermophysics*, **49**, 1229−1233.

Fabbri, A., Fen-Chong T., and Coussy O. (2006) Dielectric capacity, liquid water content, and pore structure of thawing−freezing materials. *Cold Regions Science and Technology*, **44**, 52 −66.

Fung, C.A.F.K and Burke, M.F. (1996) Investigation of the behaviour of water on the surface of modified silica using differential scanning calorimetry. *Journal of Chromatography A*, **752**, 41−57.

Gates, W., Bouazza, M., and Churchman, G. (2009) Bentonite clay keeps pollutants at bay. *Elements*, **5**, 105−110.

Höhne, G.W.H., Hemminger, W.F., and Flammersheim, H.-J. (2003) *Differential Scanning Calorimetry*. Springer-Verlag, Berlin, Heidelberg, New York.

Homshaw, L.G. (1980) Freezing and melting temperature hysteresis of water in porous materials: Application to the study of pore form. *European Journal of Soil Science*, **31**, 399−414.

Homshaw, L.G. and Cambier, P. (1980) Wet and dry pore size distribution in a kaolinitic soil before and after removal of iron and quartz. *European Journal of Soil Science*, **31**, 415−428.

Horiguchi, K. (1985) Determination of unfrozen water content by DSC. *Proceedings of the 4th International Symposium on Ground Freezing*, Sapporo, Japan, Vol. 1. A.A. Balkema, Rotterdam, pp. 33−38.

Ishikiriyama, K., Todoki, M., Min, K.H., Yonemori, S., and Noshiro, M. (1996) Thermoporosimetry: Pore size distribution measurements for microporous glass using differential scanning calorimetry. *Journal of Thermal Analysis*, **46**, 1177−1189.

Iza, M., Woerly, S., Danumah, C., Kaliaguine, S., and Bousmina, M. (2000) Determination of pore size distribution for mesoporous materials and polymeric gels by means of DSC measurements: thermoporometry. *Polymer*, **41**, 5885−5893.

Kaneko, K. (1994) Determination of pore size and pore size distribution: 1. Adsorbents and catalysts. *Journal of Membrane Science*, **96**, 59−89.

Montes, G., Duplay, J., Martinez, L., and Mendoza, C. (2003) Swelling−shrinkage kinetics of MX80 bentonite. *Applied Clay Science*, **22**, 279− 293.

Neffati, R. and Rault, J. (2001) Pore size distribution in porous glass: fractal dimension obtained by calorimetry. *The European Physical Journal B*, **21**, 205−210.

Nevzorov, A.N. (2006) Internal mechanism of metastable liquid water crystallization and its effects on intracloud processes. *Izvestiya, Atmospheric and Oceanic Physics*, **42**, 765−772.

Opitz, A., Scherge, M., Ahmed, S.I.-U., and Schaefer, J.A. (2007) A comparative investigation of thickness measurements of ultra-thin water films by scanning probe techniques. *Journal of Applied Physics*, **101**, 6064310.

Price, D.M. and Bashir, Z. (1995) A study of the porosity of water plasticised polyacrylonitrile films by thermal analysis and microscopy. *Thermochimica Acta*, **249**, 351−366.

Ravikovitch, P., Wei, D., Chueh, W.T., Haller, G.L., and Neimark, A.V. (1997) Evaluation of pore structure parameters of MCM-41 catalyst supports and catalysts by means of nitrogen and argon adsorption. *Journal of Physical Chemistry*, **101**, 3671−3679.

Rigacci, A., Achard, P., Ehrburger-Dolle, F., and Pirard, R. (1998) Structural investigation in monolithic silica aerogels and thermal properties. *Journal of Non-Crystalline Solids*, **225**, 260−265.

Rouquerol, J., Avnir, D., Fairbridge, C.W., Everett, D.H., Haynes, J.M., Pernicone, N., Ramsay, J.D.F., Sing, K.S.W., and Unger, K.K. (1994) Recommendations for the characterization of porous solids (Technical Report). *Pure and Applied Chemistry*, **66**, 1739−1758.

Salles, F., Beurroies, I., Bildstein, O., Jullien, M., Raynal, J., Denoyel, R., and Van Damme, H. (2008) A calorimetric study of mesoscopic swelling and hydration sequence in solid Na-montmorillonite. *Applied Clay Science*, **39**, 186−201.

Stepkowska, E.T., Pérez-Rodríguez, J.L., Maqueda C., and Starnawska, E. (2004) Variability in water sorption and in particle thickness of standard smectites. *Applied Clay Science*, **24**, 185−199.

Swenson, J., Elamin, K., Jansson, H., and Kittaka, S. (2013) Why is there no clear glass transition of confined water? *Chemical Physics*, **424**, 20−25.

Titulaer, M.K., Van Miltenburg, J.C., Jansen, J.B.H., and Geus, J.W. (1995) Thermoporometry applied to hydrothermally aged silica hydrogels. *Recueil Des Travaux Chimiques Des Pays Bas*, **114**, 361−370.

Torralvo, M.J., Grillet, Y., Llewellyn, P.L., and Rouquerol, F. (1998) Microcalorimetric study of argon, nitrogen, and carbon monoxide adsorption on mesoporous Vycor glass. *Journal of Colloid and Interface Science*, **206**, 527−531.

Turov, V.V. and Leboda, R., (1999) Application of ^{1}H NMR spectroscopy method for determination of characteristics of thin layers of water adsorbed on the surface of dispersed and porous adsorbents. *Advances in Colloid and Interface Science*, **79**, 173−211.

Velde, B., Moreau, E., and Terribile, F. (1996) Pore networks in an Italian vertisol: quantitative characterization by two dimensional image analysis. *Geoderma*, **72**, 271−285.

Yang Tao, Xiao-Dong Wen, Junfen Li, and Liming Yang (2006) Theoretical and experimental investigations on the structures of purified clay and acid-activated clay. *Applied Surface Science*, **252**, 6154−6161.

Zuber, B. and Marchand, J. (2000) Modeling the deterioration of hydrated cement systems exposed to frost action. Part 1: Description of the mathematical model. *Cement and Concrete Research*, **30**, 1929−1939.